# Experimental study and numerical simulation on fly ash separation with different plate voltages in rotary triboelectrostatic separator

## Ling Zhang [1], Youjun Tao [1,2], Dongping Tao [3], Weichi Zhang [1], Lu Yang [1]

[1] School of Chemical Engineering and Technology, China University of Mining and Technology, Xuzhou 221116, Jiangsu, China

[2] Key Laboratory of Coal Processing and Efficient Utilization of Ministry of Education, China University of Mining and Technology, Xuzhou, 221116, Jiangsu, China

[3] School of Mining Engineering, University of Science and Technology Liaoning, Anshan, 114051, Liaoning, China

Corresponding author: tyj05160@163.com (Youjun Tao)

**Abstract:** As the main solid wastes of coal-fired power plants, fly ash particles with different electrical properties are usually recycled using triboelectrostatic separator. The purpose of this study was to investigate the effect of different plate voltages on the separation of fly ash in a rotary triboelectrostatic separator with experiments and numerical simulation. The maximum values of yield of ash products (48.30%), and decarbonisation rate (50.89%) and the minimum loss-on-ignition (6.61%) were obtained when the plate voltage was 24 kV in the separation experiments, while 55.98%, 59.46%, 5.80% were reached respectively when the plate voltage was 26 kV in the simulation. In general, experimental data were similar with numerical simulation. The turning points appeared around 25 kV due to the increasing mismatch in products, which resulted from the reinforced rebound phenomena, namely the charged particle rebound from the electrode plate with a larger reflection velocity, when the plate voltage increased from 18 to 28 kV. It was validated by the numerical simulation results.

*Keywords:* Fly ash, rotary triboelectrostatic separator, plate voltage, numerical simulation

## 1. Introduction

Fly ash is the main solid waste of coal-fired power plants and heating boilers. In 2015, China's fly ash yield reached 570 million Mg, which causes serious threat to eco-environment and human health. However, fly ash is mainly composed of unburned carbon and oxides ($SiO_2$, $Al_2O_3$, $Fe_2O_3$, etc.), which are valuable resources from the view of mineral processing. Usually, less than 15% unburned carbon exists in fly ash and can be recycled back to a burner as a reusing fuel, which avoids the energy waste. Loss-on-ignition (LOI) represents the percentage of organic composition, which is used to evaluate the quality of fly ash. On the premise of meeting national standard of secondary class fly ash (LOI≤8%, -0.045 mm≥75%) in China (GB/T1596-2005), fly ash after decarbonisation can be used for building, road construction and other function materials. Wet and dry separation techniques are the basic decarbonisation process of fly ash. Flotation as a representative of wet separation, has been mainly used to collect the unburned carbon since 1970s (Altun et al., 2009; Zhang and Honaker, 2015). Hurst and Styron (1978) had filed a patent about recycled carbon, cenospheres and other commercial minerals based on wet flotation process. Column flotation was adopted to remove unburned carbon from municipal solid waste fly ash, and concentrates containing 5.24% unburned carbon were obtained with 61.2% removal rate (Huang et al., 2003). Compared to wet separation, dry separation has the biggest advantage of avoiding complicate dewatering process. Take advantage of electrical property difference of fly ash (Mohanta et al., 2016), triboelectrostatic separation (Dwari and Rao, 2009) as a representative of dry separation is widely used in industry. Charge generated in contact and friction process between particles and friction materials is different from the corona charging and inductive charging in

conventional electrostatic separation. In general, the triboelectrostatic separation process is simple, economic and environmental.

The charge-to-mass ratio and charge polarity were critical among all the electrical properties (Zhang et al., 2005). The charge polarity of fly ash was varied from the humidity, temperature, friction material and so on, and the charge-to-mass ratio was connected with the work function, friction area, friction frequency etc. Either uneven or opposite charge generated and transferred between friction material and particles with different dielectric constants, electrical conductivities and resistances, also constituted the presupposition for electric separation. A rotary triboelectrostatic separator (RTS) was introduced to separation of coal and phosphates, and its separation effect under different parameters was studied (Tao et al., 2009, 2010, 2011). The principle of rotary triboelectrostatic separation was discussed and the optimal separation parameters of fly ash were obtained (Tao et al., 2014, 2016). Surface charge densities of coal-silica mixtures were enhanced using the rotary triboelectrostatic separator (Chen et al., 2015).

It is well known that particles are the primary elements for mineral separation, and triboelectrostatic separation is no exception (Li et al., 2012). Separation of fly ash particles can be supposed to aggregation of particles with the same electrical properties. Therefore, tracking particles and their trajectories could help us to understand i) how electric field force affected the charged particle, ii) the difference of the positive and negative charged particles' motion, iii) the effect of mismatch phenomenon on yield, etc. Conventional measurements to track particle's motion trajectory include high-speed visualization (Wang et al., 2014) and particle image velocimetry (Mühlich et al., 2016). However, it is difficult to observe particle's motion in RTS for the opacity of friction material which is made of stainless steel. In this paper, numerical simulation is employed to describe the particle's motion trajectory. The Fluent software is a widely used computational fluid dynamics (CFD) software to represent the fluid field. It also contains many functional modules which are applied to solve different problems. The discrete phase model (DPM) module is a specified part to solve particle's motion in gas-solid flow of low concentration.

The present research focuses on the effect of different plate voltages on separation of fly ash in the rotary triboelectrostatic separator. The fundamental character of fly ash was analyzed to build the different particles models which were used in simulation. Particle's trajectories in the RTS under different plate voltage were described by the Fluent software with the DPM module.

## 2. Materials and methods

### 2.1 Materials

Fly ash samples were collected from the coal-fired power plant in Shandong Province, China. The samples of fly ash, pure ash and different sizes of fly ash for were prepared for experiments. In the first stage, the collected fly ash was dried in drying oven at 105 °C for 2 h, cooled in a vacuum chamber, and weighted 150±0.5 g for each sample. In the second stage, fly ash was placed in a muffle furnace at 1050 °C for 30 minutes, then cooled in vacuum chamber, weighted and collected as the pure ash samples, which were the products after removing all the organic composition of fly ash. In the third stage, the prepared fly ash samples were screened to +0.125mm, -0.125+0.074mm, -0.074+0.045mm and -0.045mm, in order to obtain different sizes of fly ash. Finally, the density of prepared samples was measured by using a pycnometric method. Parameters of experimental samples are showed in Table 1.

Table.1. Yield, loss-on-ignition (LOI) and density of fly ash samples

| Size, mm | Yield, % | LOI, % | Density, $kg \cdot m^{-3}$ |
|---|---|---|---|
| +0.125 | 7.68 | 7.38 | 2580.64 |
| -0.125 ~ 0.074 | 14.97 | 8.27 | 2571.89 |
| -0.074 - 0.045 | 17.57 | 11.41 | 2541.02 |
| -0.045 | 59.79 | 12.55 | 2529.81 |
| Total | 100 | 11.31 | 2542.03 |

### 2.2 Triboelectric separation equipment

The rotary triboelectric separator (RTS) consists of airflow-in chamber (Section I), rotary triboelectrostatic chamber (Section II) and electrical separation chamber (Section III), as shown in Fig.1. Section I is the area where airflow brings the feeding particles into the separator. Section II, which consists of friction roller and chamber wall, is used to generate charge. The high-speed rotating friction roller increases the number of particle-chamber wall and particle-friction roller contacts, which is helpful to generate more charge in the friction process. Section III is composed of negative and positive electrode plates. In the uniform electric field, which is formed between the electrode plates, particles with opposite charge move to different electrode plate and separate under the Lorentz force.
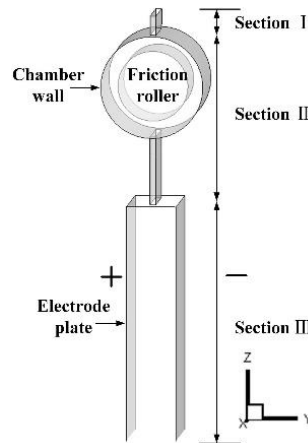


Fig. 1. Scheme of RTS

### 2.3 Fly ash separation

The electrical separation experiments were designed to study the separation effect. Plate voltage was the considered factor. A small-scale vibrator feeder (GVZ-2) was the feeding equipment which gave security for the mass rate. High voltage direct current power (J50S5RC) supplied stable plate voltage from 0 to 35 kV. The friction roller was driven by a three-phase asynchronous motor (Y2-802-4) through pulley. Three air exhausters (YLW77-15) were used to supply steady air flow. Separation parameters were as follows: rotating speed of rotary friction roller of 189.95 rad/s, feeding rate of 0.61 g/s (which corresponds to vibrational frequency 22 Hz), exhausting rate caused by three air exhausters i.e. $3.14\times10^{-4}$, $3.14\times10^{-4}$, $3.14\times10^{-4}$ m$^3$/s, plate voltage of 18, 20, 22, 24, 26 and 28 kV. Three products (concentrate, middling and tailing) were collected after separation. The yield and loss-on-ignition (LOI) were calculated. The size composition of products under different plate voltages were measured by a laser particle size analyzer (Microtrac S3500).

### 2.4 Elemental analysis

An X-ray fluorescence analyzer (XRF, S8 Tiger, Bruker) was employed to measure the component and distribution of fly ash.

### 2.5 Fly ash surface profile measurements

The scanning electron microscope (SEM, Quanta 250) and polarization microscope (Motic BA310Pol) were employed to illustrate the surface profile and sizes of fly ash. Image processing was applied to calculate the shape factor of different particles based on the polarized image. The shape factor was a key element in simulation, which represented the volume and surface character of real ash particle. Three pictures of dispersive fly ash were collected to calculate the shape factor. The captured figures of fly ash were divided into a lot of segments, and each segment represented one particle. Then, the area and perimeter of each particle was calculated. The surface shape factor was a result of dividing the area into the perimeter.

**2.6 Evaluation index of separation**

The purpose of fly ash separation is to decrease the carbon content and obtain high ash products, so concentrates are the ash products which have low LOI and can be used for construction materials. The yield, LOI and decarbonisation rate are the basic product indicies. The yield is expressed as:

$$\gamma_c = \frac{m_c}{m_{feed}} \times 100\%.$$ (1)

The decarbonisation rate (D) is used to reveal the separation effect of fly ash and it reflects the decrease of unburned carbon before and after separation, and is expressed as:

$$D = \frac{\gamma_c(100-LOI_c)}{100-LOI_{feed}} \times 100\%.$$ (2)

In Eqs. 1 and 2, $m_c$ is the mass of concentrate, $m_{feed}$ is the mass of feed, $LOI_c$ is the LOI of concentrates, $LOI_{feed}$ is the LOI of fly ash.

**2.7. Numerical simulation method**

Materials of friction roller, friction chamber and electrode plate are made of stainless steel, therefore it is difficult to observe the motion status of fly ash particles. In order to visualize the effect of particles' motion on separation results, numerical simulation using Fluent 14.5 software as adopted. Two specified modules: discrete phase module (DPM) and magnetohydrodynamics module (MHD) were applied to show the trajectories of particles. DPM was the module for tracking particles' motion in RTS with low feed concentration, and MHD was to reveal the charged particles' motion behavior under the added electric field force.

This simulation was conducted with generating structured meshes, setting parameters, numerical calculation and post processing in sequence. Structured meshes were generated by ICEM software (Fig. 2). Standard *k-ε* Model was chosen as the turbulence model in simulating dynamic airflow. Inert ash particles and carbon particles representing +0.125mm, -0.125+0.074mm, -0.074+0.045mm and -0.045mm were released from the inlet. High voltage was appended between the positive electrode plate and negative electrode plate. All the wall boundaries were coarse with 0.3 roughness height and 0.5 roughness constant. Shape factors of three fly ash samples were 0.66, 0.62, 0.60, and their average 0.63 was adopted. The electrical conductivity of air, ash particle and carbon particle were $3\times10^{-9}$ s/m, $3.57\times10^{-9}$ s/m and 52.6 s/m, respectively. A semi-implicit method for the pressure linked equation (SIMPLEC) solution method was used to accomplish the final iterative computations. Inert particles were tracked in sequence after residuals reached the convergence condition. Finally, airflow distribution and particles' trajectory parameters were exported and analyzed in other software. The main parameters used in the simulation are listed in Table 2.
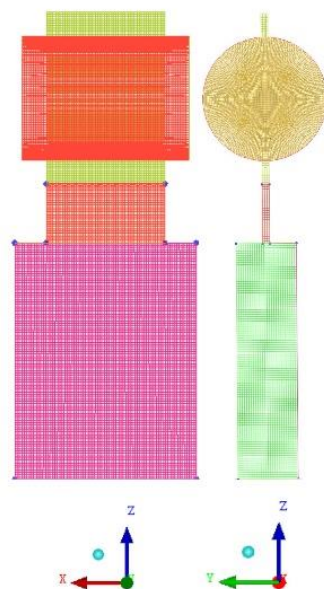


Fig. 2. Computational meshes of RTS

Table 2. Parameters of simulation

|  | Parameters | value |
|---|---|---|
| Simulation model | Viscous model | k-epsilon |
|  | Inlet airflow velocity (m/s) | 1.05 |
|  | Rotating angular velocity (rad/s) | 189.95 |
|  | Wall roughness height (mm) | 0.3 |
|  | Wall roughness constant | 0.5 |
|  | Solution method | SIMPLEC |
| DPM (Injection particles) | Diameter (mm) | +0.125, 0.125-0.074, 0.125-0.045, -0.045 |
|  | Ash particle percentage (%) | 7.68, 14.97, 17.57, 59.79 |
|  | Average ash particle density (kg · m⁻³) | 2653 |
|  | Carbon particle diameter (mm) | +0.125, 0.125-0.074, 0.125-0.045, -0.045 |
|  | Carbon particle percentage (%) | 7.68, 14.97, 17.57, 59.79 |
|  | Average carbon particle density (kg · m⁻³) | 1670 |
|  | Velocity (m/s) | 1.05 |
|  | Shape factor | 0.63 |
| MHD | Plate voltage (KV) | 18, 20, 22, 24, 26, 28 |
|  | Electrical conductivity of air (s/m) | $3 \times 10^{-9}$ |
|  | Electrical conductivity of ash particle (s/m) | $3.57 \times 10^{-9}$ |
|  | Electrical conductivity of carbon particle (s/m) | 52.6 |
|  | Saturation charge density of ash particle (c/m³) | -0.009413, -0.016806, -0.027266, -0.096427 |
|  | Saturation charge density of carbon particle (c/m³) | 0.009413, 0.016806, 0.027266, 0.096427 |
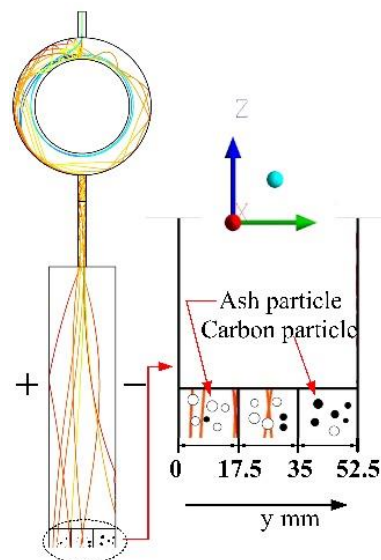


Fig. 3. Calculation methods of products index in simulation

Fig. 3 shows the calculation methods of products index in simulation. The yield, LOI and decarbonisation rate were calculated as follows:

$$\gamma_C = \frac{N_{A1(0-35mm)}*m_{A1}+N_{A2(0-35mm)}*m_{A2}+\cdots\cdots+N_{C4(0-35mm)}*m_{C4}}{m_{Total}} \times 100\% \tag{3}$$

$$\text{LOI}_C = \frac{N_{C1(0-35mm)}*m_{C1}+N_{C2(0-35mm)}*m_{C2}+N_{C3(0-35mm)}*m_{C3}+N_{C4(0-35mm)}*m_{C4}}{m_{Total(0-35mm)}} \times 100\% \tag{4}$$

$$D = \frac{\gamma_c(100 - LOI_c)}{100 - LOI_{feed}} \times 100\% \qquad (5)$$

where $N_{A1}$, $N_{A2}$, $N_{A3}$, $N_{A4}$, $N_{C1}$, $N_{C2}$, $N_{C3}$ and $N_{C4}$ represent the number of particles in products, that is +0.125mm ash particles, 0.125 - 0.074mm ash particles, 0.074 - 0.045mm ash particles, -0.045mm ash particles, +0.125mm carbon particles, 0.125-0.074mm carbon particles, 0.074-0.045mm carbon particles and -0.045mm carbon particles, respectively. $m_{A1}$, $m_{A2}$, $m_{A3}$, $m_{A4}$, $m_{C1}$, $m_{C2}$, $m_{C3}$ and $m_{C4}$ represent the mass of particles as state above, $N_{Ci(0-35mm)}$ represents the number of particles appeared between 0 and 35mm in y direction, $m_{Total}$ and $m_{Total(0-35mm)}$ are the total mass and total mass at 0-35mm of products.

## 3. Results and discussion

### 3.1 Component and surface profile characteristics of fly ash

XRF results presented in Table 3 show that fly ash had 38.95% $SiO_2$, 25.24% $Al_2O_3$, 16.12% CaO and 4.94% $Fe_2O_3$, which belonged to silico-aluminate fly ash. The SEM photos showed that the fly ash particles were below 150 μm. Most of these particles were irregular and covered with chippings (Fig. 4). The polarization microscope was applied to measure the surface profile of fly ash in general (Figs. 5-7). Branching, overlapping, connecting and mixing were the main distribution patterns. Agglomeration often appeared between small particles because they had high surface energy due to their large specific surface area. Fig. 6(a) showed that the agglomerated particles attached to either large particles or cluster of large agglomerated particles and became branches. Fig. 6(b) showed the common overlapping phenomenon, where large number of particles covered each other. Fig. 6(c) represented the connecting phenomenon of two particles combined into one. Fig. 6(d) showed the common mixing state of either different particles or clusters. Assumed the fly ash particles as carbon particle and $(SiO_2)x$-$(Al_2O_3)y$ particles, these particles existed either independently or covered each other as shown in Fig. 7. Diverse distribution between particles had an influence on the charge density and polarity, which affected the separation effect of fly ash.

Table 3 Chemical composition of fly ash

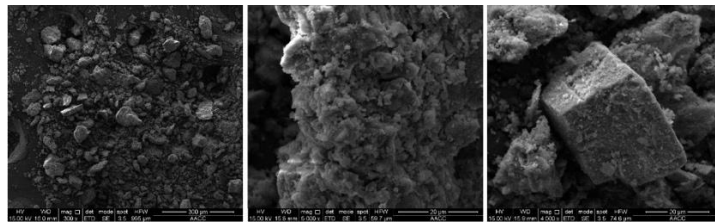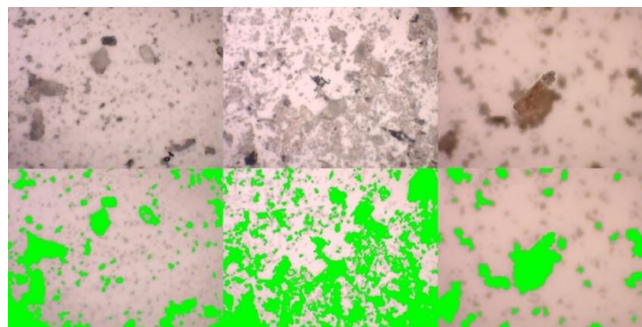| Ingredients | $SiO_2$ | $Al_2O_3$ | CaO | $CO_3$ | $Fe_2O_3$ | S | K | Mg | Ti | Others |
|---|---|---|---|---|---|---|---|---|---|---|
| Mass fraction, % | 38.95 | 25.24 | 16.12 | 10.10 | 4.94 | 1.74 | 1.08 | 0.88 | 0.57 | 10.49 |



Fig. 4. SEM photos of fly ash
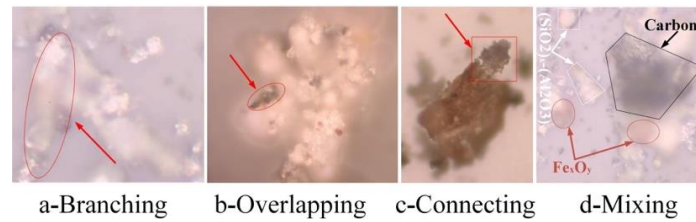


Fig. 5. Divided segments of fly ash
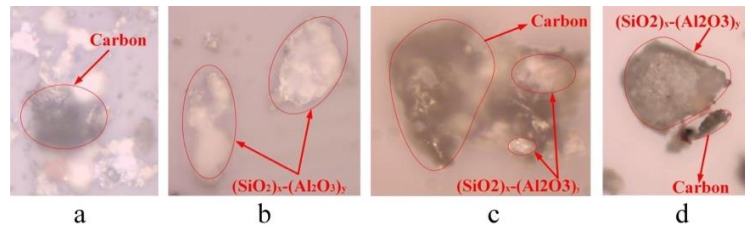
Fig. 6. Distribution characteristics of fly ash



Fig. 7. Surface characteristics of carbon and ash particles

## 3.2 Separation results of fly ash

Fig. 8 showed that the yield of concentrates increased from 38.23% to the maximum value of 48.30%, when the plate voltage increased from 18 to 24 kV, but the yield slightly decreased while the voltage increased to 28 kV. It was dangerous that the air breakdown would happen when the plate voltage exceeded 30 kV, so the maximum plate voltage was set to 28 kV. LOI of concentrates decreased from 7.61% to the minimum 6.61% when the plate voltage increased from 18 to 24 kV, then it increased when the plate voltage increased from 24 to 28 kV. The trend of decarbonisation rate varied with plate voltage and it was in accord with the yield. The decarbonisation ratet reached the maximum 50.89% when the plate voltage was 24 kV. The turning point at 24 kV should be focused for its maximum yield and minimum LOI. When the plate voltage increased from 18 to 24 KV, the electric field intensity increased from $3.53 \times 10^2$ to $4.71 \times 10^2$ kV/m, and the Lorentz force imposed on particles increased directly. The negatively charged ash particle shifted to the positive plate became concentrates and the positively charged carbon particle to the negative plate became tailings gradually with the increase in the Lorentz force. When the plate voltage increased from 24 to 28 kV, it was interesting that the yield of concentrates began to decrease and the LOI to increase. The explanation is that with the electric field intensity increased to $5.49 \times 10^2$ kV/m, it was unavoidable that ash and carbon particles collided with the electrode plate for the large electric field intensity. Collisions between particles were indistinctive because the volume fraction of particles in experiments was less than 10%. Collisions between particles and electrode plate must be taken into account. The greater the electric field intensity, the bigger the impact velocity. The charge neutralized once the particles collided with the electrode plate, but the collision of particles continued. The neutralized particle began to rebound without the influence of Lorentz force which led to the change of yield and LOI.
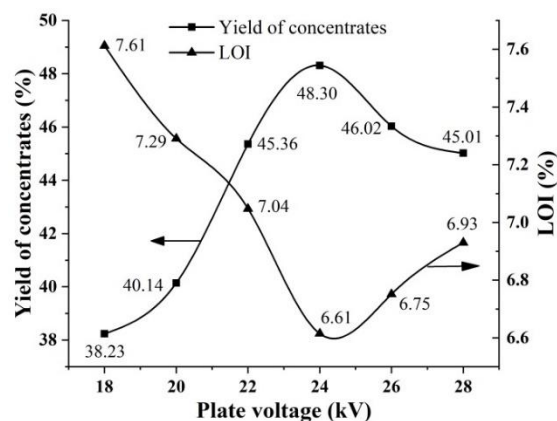


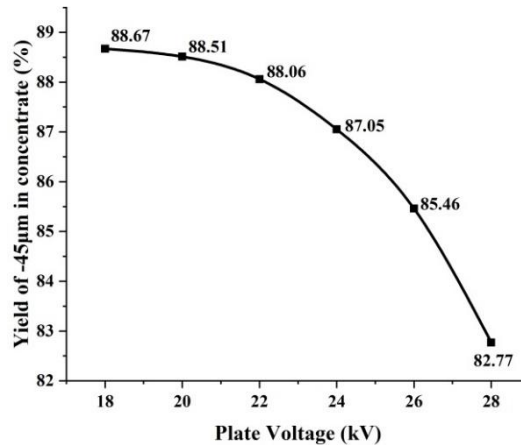Fig. 8. Yield and LOI vs. plate voltage of experiments

Fig. 9. Yield of -45 µm size fraction in concentrate vs. plate voltage of experiments

The yield of -45 µm size fractiom in concentrates decreased from 88.67% to 82.77% with the increase of plate voltage and conformed to the size standard of secondary class fly ash (-0.045mm≥75%), which is shown in Fig. 9. LOI of concentrates were between 5.80 and 7.06% when the plate voltage was 22-28 kV, which is in accordance with the LOI standard of secondary class fly ash (LOI≤8%).

### 3.3 Analysis of simulation results

Fig. 10 represents the yield and LOI of negative electrode plate (abbreviated to NEP) products what corresponds to the ash products in experiments. The yield of NEP products increased to the maximum of 50.72% with the plate voltage increase to 26 kV, then it slightly decreased. The LOI of NEP products decreased from 8.89% to 5.57% when the plate voltage increased from 18 to 26 kV, and then increased to 7.02% when the voltage was 28 kV. Fig.11 shows the decarbonisation rate of experiments and simulation. The decarbonisation rate first increased, and then decreased when the plate voltage increased from 18 to 28 kV. The maximum decarbonisation rate of 50.89% was obtained at the plate voltage of 24 kV in experiments, and 50.89% was obtained at 26 kV in simulation. The trends between simulation and experiments agreed well, while the simulation results were higher for about 5~10%. In simulation, ash and carbon particles were assumed as pure ones and their motion and charging characteristics were uniform and regular than the real ash particles what meant the simulation was thorough and perfect. Meanwhile, inclusion and overlap were the common phenomena to real ash particles which led to the surface charge uneven distributed, but they scarcely emerged between ash particles and carbon particles in simulation. Based on above, the simulation process was thorough than the experiment, so the distinction happened.

The decarbonisation rate increased with the increase in the plate voltage, then decreased, and had a peak when the plate voltages were 24 and 26 kV in experiments and simulation, respectively. As shown in Section 3.2, particles moved to the positive electrode plate might rebounded and became middle products or carbon products, it was obvious for larger particles. Larger particles had more chance to get charge than smaller particles due to the larger surface area. They would obtain larger incident velocity and reflection velocity, which led to the change of products. Fig. 12 shows trajectories of +0.125mm ash particles which was rereleased from the center of inlet for different plate voltages. The particle deflected in negative y axis direction under the effect of Lorentz force when the plate voltage varied from 18 to 20 kV. Because the Lorentz force imposed on the particle was not large enough, the particle came out directly as the ash or middle products without colliding with the positive plate. The particle began to collide with the positive plate due to the increase of Lorentz force exerted on particle when the plate voltage varied from 22 to 28 kV. The particle had a rebound velocity vector in positive y axis direction, which meant the ash particle might become the middle, carbon or ash products. The rebound behavior caused by collision made the distribution of products complex and led to change in the decarbonisation rate. The length of Section Ⅲ also had an impact on the rebound phenomena. However, the length of

Section III in simulation was the same as the RTS equipment. The comparison of separation results between simulation and experiments could be implemented.
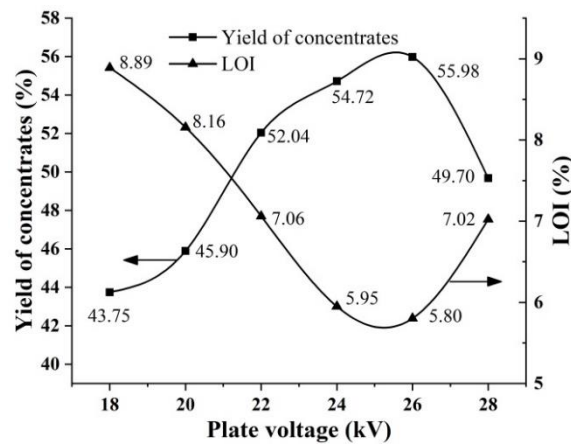


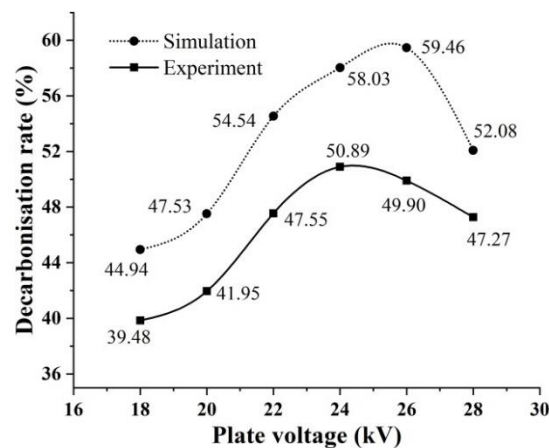Fig. 10. Yield and LOI vs. plate voltage of simulation



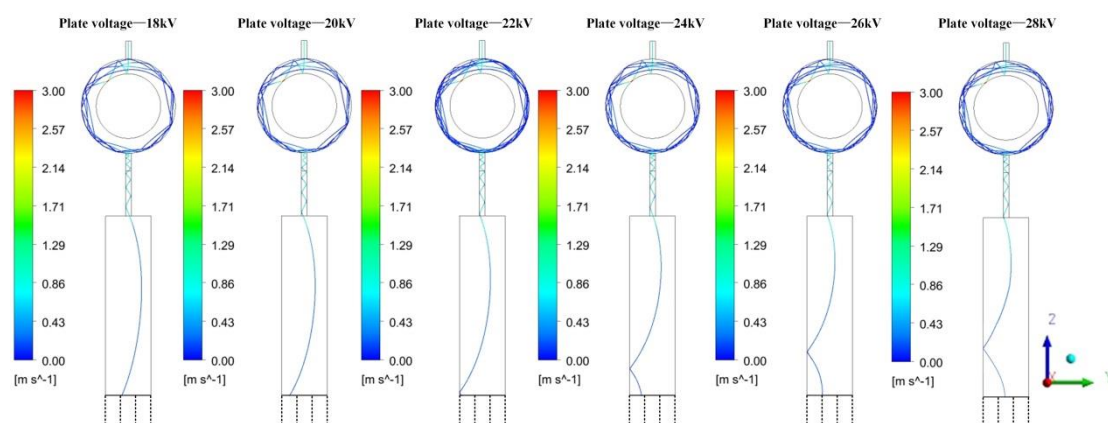Fig. 11. Decarbonisation rate of experiments and simulation



Fig. 12. Trajectories of +0.125mm ash particles under different plate voltages

## 4. Conclusions

Separation of fly ash using a rotary triboelectrostatic separator under different plate voltages was studied by a comparison of experiments and numerical simulation. The fundamental physical parameters of fly ash were studied by a modern analytical technique which revealed the effect on separation from the view of raw material. It can also be helpful to build a basic particle model in

simulation. Plate voltage had a significant effect on the decarbonisation efficiency. The decarbonisation rate first increased, then decreased with the increase of plate voltage from 18 to 28 kV. The maximum values of yield of ash products (48.30%), and decarbonisation rate (50.89%) and the minimum loss-on-ignition (6.61%) were obtained when the plate voltage was 24 kV. The concentrates reached the standard of secondary class fly ash when the voltages were 22-28 kV. The numerical simulation results were in accordance with the experiments in general with separation results of 55.98% (maximum yield), 59.46% (maximum decarbonisation rate), 5.80% (LOI) when the plate voltage was 26 kV. The turning point of separation appeared in experiments and simulation when the plate voltage was around 25 kV. It was due to the reinforcing rebound phenomena between particles and electrode plate with the increase of plate voltage. This also be validated by the trajectories of +0.125mm ash particles for the plate voltage from 18 to 28 kV. By contrast, simulation can be an effective method to forecast the separation effect of fly ash with accurate parameters.

**References**

ALTUN, N. E., XIAO, C., AND HWANG, J. Y., 2009. *Separation of unburned carbon from fly ash using a concurrent flotation column*. Fuel Process. Technol., 90(12), 1464-1470.

CHEN, J., HONAKER, R., 2015. *Dry separation on coal–silica mixture using rotary triboelectrostatic separator*. Fuel Process. Technol., 131, 317-324.

DWARI R. K., RAO K. H., 2009. *Fine coal preparation using novel tribo-electrostatic separator*. Miner. Eng., 2009, 22(2):119-127.

DANIEL, T., FAN, M. M., JIANG, X. K., 2009. *Dry coal fly ash cleaning using rotary triboelectrostatic separator*. Min. Sci. Tech., 19(5), 642-647.

DANIEL, T., MOHAMMAD, A.H., 2010. *Beneficiation study of Eshidiya phosphorites using a rotary triboelectrostatic separator*. Min. Sci. Tech., 20(3), 357-364.

DANIEL, T., SOBHY, A., LI, Q., HONAKER, R., ZHAO, Y., 2011. *Dry cleaning of pulverized coal using a novel rotary triboelectrostatic separator (RTS)*. Int. J. Coal Prep. Util., 31(3-4), 187-202.

LI, H. S., ZHANG, X. X., CHEN, Y. H., 2012. *Collision characteristics of particles in the friction device of triboelectrostatic separator*. J. China U. Min. Technol., 41(4), 607-612.

HURST, V. J., STYRON, R. W., 1978. *Fly ash beneficiation process*. U.S. Patent No. 4,121,945.

HUANG, Y., TAKAOKA, M., TAKEDA, N., 2003. *Removal of unburned carbon from municipal solid waste fly ash by column flotation*. Waste Manage., 23(4), 307-313.

MÜHLICH, P., CASE, W., HÖRMANSPERGER, J., BEYRER, M., WINDHAB, E. J., 2016. *Particle image velocimetry (PIV) in food powders during vacuum-steam-vacuum (VSV) treatment*. Powder Technol., 299, 1-8.

MOHANTA, S. K., ROUT, B., DWARI, R. K., REDDY, P. S. R., MISHRA, B. K., 2016. *Tribo-electrostatic separation of high ash coking coal washery rejects: Effect of moisture on separation efficiency*. Powder Technol., 294, 292-300.

WANG H., CHEN S., CAI B., GE L., CHEN Q., 2014. *Triboelectric Separation Study on the Dynamics of Tribocharged Coal and Mineral Particles in Free-Fall Triboelectric Separator*. Sep. Sci. Technol. 49(18):2990-2998.

TAO Y., ZHU X., TAO D., DENG M., ZHANG X., 2016. *Optimization of triboelectrostatic decarbonization experiment of fly ash by Design-Expert*. J. China coal Soc., 41(2), 475-482.

TAO Y., ZHANG, J., WANG, X., DENG, M., TAO, D., 2014. *Study of rotary triboelectrostatic separation and decarbonization of fly ash*. J. China U. Min. Technol., 43(4), 672-677.

ZHANG, W., HONAKER, R., 2015. *Studies on carbon flotation from fly ash*. Fuel Process Technol., 139, 236-241.

ZHANG, X. X., DUAN, C. H., FENG-QIN, Y. U., GAO, M. H., JING-MIN, H. E., 2005. *Electric property and tribocharging of fine coal*. J. China U. Min. Technol., 34(6), 694-697.